Check for updates

Expanding proton-insertion coupled electron transfer into tungsten oxides to non-aqueous organic acid electrolytes

Saeed Saeed, [a] Zhou Lu, [b] Ellen M. Matson [b] and Veronica Augustyn *[a]

We investigated proton insertion-coupled electron transfer (PICET) into tungsten oxide films using non-aqueous organic acid electrolytes. *Operando* UV-vis-NIR spectroelectrochemistry confirms PICET, showing respective broadband and dual-band transmittance changes for WO_3 and $WO_3 \cdot H_2O$ in the visible and NIR regions. $WO_3 \cdot H_2O$ retains facile PICET kinetics in the absence of water.

The ability of transition metal oxides (TMOs) to undergo electrochemical proton-coupled electron transfer (PCET) reactions renders them useful as electrodes for electrochemical energy storage and as electrocatalysts for electrochemical synthesis.[1–3] Despite this broad application space, most studies of electrochemical PCET with TMOs have been limited to conditions where the electrolyte is a strong acid or base in water. While this can lead to facile interfacial and mass transport kinetics, it limits fundamental understanding of PCET in TMOs to conditions at the extremes of the pH scale and in water. On the other hand, investigations of PCET in polyoxometalates, considered as molecular-scale analogs of TMOs, typically utilize non-aqueous solvents and organic acids to explore electrochemical PCET reactivity with proton donors over a broad pK_a range.[4–6] The nature of the electrolyte proton donor is important as it influences both the thermodynamics and kinetics of the PCET reaction. Reports on electrochemical PCET into TMOs from non-aqueous electrolytes are limited but include TiO_2 and $VO_2(B)$[7,8] and NiO and CeO_2.[9–11]

Here, we investigate the electrochemical PCET reactivity of a model TMO, WO_3, and its hydrated, Brønsted acid relative, $WO_3 \cdot H_2O$, in organic acids in a non-aqueous solvent. Like other early TMOs, tungsten oxides can undergo PCET reactions at the surface followed by accommodation of the protons within the oxide bulk, a process termed proton-insertion coupled electron transfer (PICET).[1,12,13] Fig. 1 shows the primary steps involved during PICET with WO_3.

Here, we provide the first report of electrochemical PICET into tungsten oxides in the absence of water using electrolytes containing organic acids in acetonitrile (MeCN) and compare the behavior to a more common inorganic aqueous acid electrolyte, 0.5 M H_2SO_4. We used cyclic voltammetry and *operando* UV-vis-NIR spectroelectrochemistry to study PICET into tungsten oxide thin films in non-aqueous electrolytes containing organic acids ranging in pK_a from 5.07 to 19.35. We found that the redox features associated with PICET shift in a Nernstian fashion. Comparing their behavior in non-aqueous *vs.* aqueous acid electrolytes, WO_3 shows slower PICET kinetics while those of $WO_3 \cdot H_2O$ remain the same. We hypothesize that the structural water in $WO_3 \cdot H_2O$ helps maintain fast interfacial PICET kinetics even in the absence of water. WO_3 and $WO_3 \cdot H_2O$ both show suppressed redox peaks in non-aqueous organic acid electrolytes, which we hypothesize occurs from kinetic limitations in the organic acid electrolyte. UV-vis-NIR spectroelectrochemistry shows that WO_3 has a single broadband change in transmission across all visible and IR wavelengths even at low states of PICET. $WO_3 \cdot H_2O$ shows dual-band behavior where low states of PICET lead to changes in the IR before activating a visible response. This study expands PICET into tungsten oxides to non-aqueous

[a] *Department of Materials Science and Engineering, NC State University, Raleigh, NC 27606, USA. E-mail: vaugust@ncsu.edu*
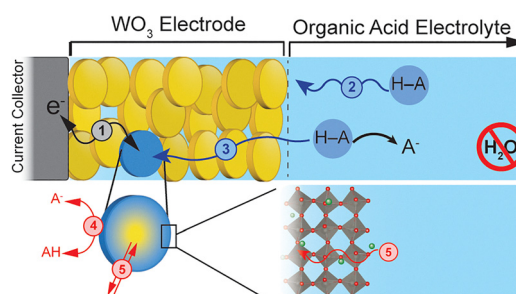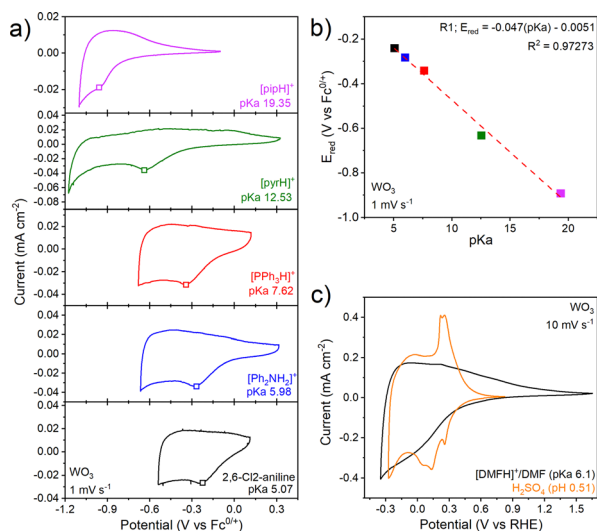[b] *Department of Chemistry, University of Rochester, Rochester, NY 14627, USA*

Fig. 1 PICET mechanism of a tungsten oxide thin film electrode in a non-aqueous organic acid electrolyte: (1) electron transport through the electrode network; mass transport of the proton donor (HA) in the (2) bulk electrolyte and (3) porous electrode; (4) PCET at the WO_3/electrolyte interface; and (5) coupled H^+/e^- transport into the WO_3 bulk.

Fig. 2 Electrochemistry of WO_3 in non-aqueous electrolytes containing organic acids ranging in pK_a from 5.07 to 19.35. (a) CVs at 1 mV s^{-1}, (b) pK_a-dependence of the first reduction peak. The red dashed line represents the linear regression fit with a slope of -47 mV pK_a^{-1} unit, (c) CVs at 10 mV s^{-1} in 0.5 M H_2SO_4 and in the non-aqueous electrolyte, 0.1 M [DMFH]$^+$/DMF buffer and 0.1 M NBu$_4$PF$_6$ in MeCN, both referenced to the RHE potential scale. Open squares in (a) denote the cathodic peak potential, E_{red}, used in (b).

electrolytes, facilitating the electrochemical conditions available for electrochemical transformations involving PCET to and from TMO surfaces.

Physical characterization of the electrodeposited $WO_3 \cdot H_2O$ and WO_3 films is shown in Fig. S4 and S5. We performed cyclic voltammetry of the WO_3 thin film electrode in non-aqueous electrolytes containing organic acids whose pK_a ranged from 5.07 to 19.35 in MeCN (Fig. 2a). Such a pK_a range is not accessible in aqueous electrolytes without dissolution of WO_3 to WO_4^{2-}. In the absence of organic acids (e.g., in 0.1 M NBu$_4$PF$_6$ in MeCN), WO_3 shows a rectangular cyclic voltammetry response as expected for non-faradaic double layer charging (Fig. S7). The presence of organic acids leads to an order of magnitude increase in the current density and broad but notable cathodic and anodic current peaks, likely from faradaic PICET. In line with this hypothesis, the cathodic peak potential, E_{red}, shows near-Nernstian dependencies of 47 mV pK_a^{-1} unit (Fig. 2b). The decrease from an ideal Nernstian process of 59 mV pK_a^{-1} unit suggests the possibility of <1H$^+$, 1e$^-$ transfer. Because of the poorly-resolved anodic features, this sub-Nernstian behavior may also be due to kinetically-limited PICET. This trend is opposite to aqueous electrolytes, where many TMOs exhibit super-Nernstian (>59 mV pK_a^{-1}) behavior.[14] The broad nature of the anodic peak prevented us from determining its pK_a dependence.

Fig. 2c shows a comparison of WO_3 in an aqueous inorganic acid electrolyte (0.5 M H_2SO_4) and a non-aqueous electrolyte containing a weak organic acid buffer, 0.1 M [DMFH]$^+$/DMF, both at 10 mV s^{-1}. We observed significantly smaller and less defined currents in the organic acid vs. the inorganic acid aqueous electrolyte, especially for the anodic sweep. To verify that our current response under non-aqueous conditions was

not limited by the concentration of the organic acid in solution, we cycled WO_3 in a non-aqueous electrolyte containing either 20 mM or 100 mM [DMFH]$^+$ (Fig. S8b). The CV showed a slight cathodic shift in the redox potential, perhaps due to drift of the Ag pseudoreference electrode. There were no other changes suggesting that the proton donor was in sufficient excess at these concentrations. At 10 mV s^{-1}, WO_3 inserts 0.2 H$^+$/e$^-$ in both 0.5 M H_2SO_4 and 0.1 M [DMFH]$^+$/DMF (Fig. 2c). In [DMFH]$^+$/DMF at 2 mV s^{-1}, WO_3 can take up to $\sim$0.25 H$^+$/e$^-$ per W, which decreases to $\sim$0.1 H$^+$/e$^-$ at 200 mV s^{-1} for a capacity retention of 47% (Fig. S10a, b and Fig. S11a). In 0.5 M H_2SO_4, the capacity retention at 200 mV s^{-1} is 60%,[15] indicating more limited PICET kinetics in the non-aqueous electrolyte. The comparison of charge as a function of potential in the aqueous and non-aqueous electrolytes at 10 mV s^{-1} is shown in Fig. S12. This comparison shows that the same amount of charge is taken up in both electrolytes, but that it occurs over a broader potential range and with larger hysteresis in the non-aqueous electrolyte. Our previous work showed that CV redox peaks in 0.5 M H_2SO_4 are associated with first-order solid state phase transitions.[16] The lack of well-defined redox peaks in the non-aqueous electrolytes indicates that PICET occurs over a broader potential window. Interfacial water is a key contributor to fast PICET kinetics in mechanistic studies of hydrogen spill-over into tungsten oxides.[17,18] We thus hypothesize that the changes in CV features in organic acid non-aqueous electrolytes vs. inorganic aqueous electrolytes for WO_3 originate from the absence of water to promote PICET at its interface.

We further quantified the PICET kinetics of WO_3 in [DMFH]$^+$/DMF by considering the relationship between the peak current (i_p) and scan rate (v) between 2–200 mV s^{-1}:

$$i_p = av^b \tag{1}$$

where a and b are constants. In a thin film insertion electrode (where solid-state mass transport distances are small), the "b-value" has boundary conditions of 0.5 for semi-infinite diffusion and 1 for surface-controlled reactions or double layer charging, whereas intermediate values can be attributed to finite diffusion.[19] The cathodic b-value for WO_3 in [DMFH]$^+$/DMF is 0.92 (Fig. S11c), which we interpret as kinetics limited by finite solid-state diffusion required for PICET into the WO_3 electrode. In aqueous acidic electrolytes, the b-value for the cathodic peak is lower, near 0.68.[20] We hypothesize that this is due to the higher degree of PICET into WO_3 at a given potential, which leads to more limited mass transport.

Next, we consider the electrochemistry of $WO_3 \cdot H_2O$ in non-aqueous electrolytes containing organic acids (Fig. 3a). In each case the CVs are similar, with a broad current response that increases upon cathodic polarization and reverses upon anodic polarization, consistent with electron transfer to a semiconducting oxide. $WO_3 \cdot H_2O$ exhibits super-Nernstian behavior, with the cathodic redox peak exhibiting a 71 mV pK_a^{-1} unit shift (Fig. 3b). The changes (Fig. 3b) in linearity suggest changes in the mH$^+$/ne$^-$ ratios at different pK_a ranges, however, further investigation is required to understand the origin of these changes. The total charge passed in $WO_3 \cdot H_2O$ corresponds to $\sim$0.06 e$^-$/H$^+$ per
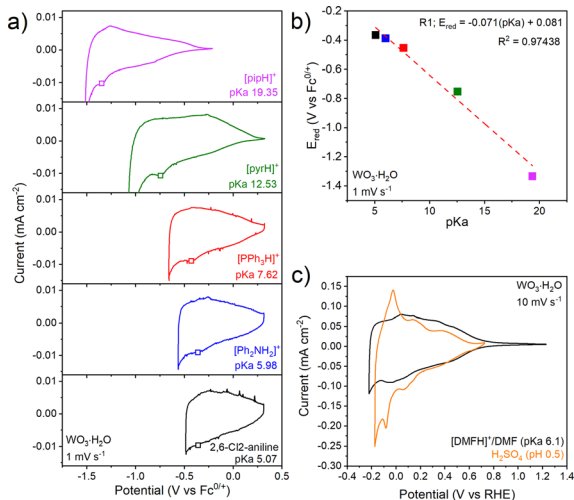
Fig. 3 Electrochemistry of $WO_3 \cdot H_2O$ in non-aqueous electrolytes containing organic acids ranging in pK_a from 5.07 to 19.35: (a) CVs at 1 mV s^{-1}, (b) pK_a-dependence of the first reduction peak potential. The red dashed line represents the linear regression fit with a slope of -71 mV pK_a^{-1} unit, (c) CVs at 10 mV s^{-1} in 0.5 M H_2SO_4 and the non-aqueous electrolyte, 0.1 M $[DMFH]^+$/DMF and 0.1 M NBu_4PF_6 in MeCN, both referenced to the RHE potential scale. Open squares in (a) denote the cathodic peak potential, E_{red}, used in (b).

Fig. 4 *Operando* electrochemical UV-vis-NIR spectra of WO_3 and $WO_3 \cdot H_2O$ collected in 0.1 M $[DMFH]^+$/DMF and 0.1 M NBu_4PF_6 in MeCN. Color map plots of normalized transmittance as a function of time for WO_3 (a) and $WO_3 \cdot H_2O$ (b) collected at 10 mV s^{-1}. Rate of transmittance change, $d\Delta T/dt$, vs. potential for WO_3 (c) and $WO_3 \cdot H_2O$ (d) collected at 10 mV s^{-1}.

formula unit in $[DMFH]^+$/DMF at 2 mV s^{-1}, with $\sim 85\%$ capacity retention at 200 mV s^{-1} (Fig. S11b). At 10 mV s^{-1} (Fig. 3c), $WO_3 \cdot H_2O$ inserts 0.06 H$^+$/e$^-$ in the organic acid-containing electrolyte, slightly lower than the 0.08 H$^+$/e$^-$ observed in H_2SO_4. Compared to H_2SO_4 (Fig. 3c), the overall CV shape of $WO_3 \cdot H_2O$ in $[DMFH]^+$/DMF is relatively similar above 0 V vs RHE. Below 0 V vs. RHE, the CV shape in the organic acid deviates from the aqueous case, showing no sharp redox peaks, as in WO_3, likely due to kinetic limitations in the electrolyte. We hypothesize that the Brønsted acidity of $WO_3 \cdot H_2O$ allows for fast interfacial PCET kinetics even in the absence of water in the electrolyte. b-value analysis of $WO_3 \cdot H_2O$ (Fig. S11d) shows $b \approx 0.99$, indicating a surface-controlled process as seen in aqueous inorganic acids.[20] Raman spectroscopy shows that neither WO_3 nor $WO_3 \cdot H_2O$ undergoes noticeable structural change after electrochemical cycling (Fig. S13).

To conclusively determine whether the electrochemical response in non-aqueous electrolytes occurs due to PICET, we performed *operando* electrochemical UV-VIS-NIR spectroscopy, since ion insertion into tungsten oxides leads to electrochromism.[13,21–23] Upon reduction in $[DMFH]^+$/DMF at 10 mV s^{-1}, WO_3 shows a decrease in transmittance between 200–390 nm and 400–1100 nm corresponding to the formation of H_xWO_3, followed by a reversible increase in transmittance during oxidation (Fig. 4a). Transmittance changes below 400 nm are associated with interband transitions from the valence band to the conduction band.[21,24] With increasing states of charge, WO_3 undergoes structural transformations from a monoclinic, to a tetragonal, to a cubic bronze structure with near-ideal WO_6 octahedral environments.[25] Overlapping low-lying d-orbitals of the higher symmetry H_xWO_3 results in simultaneous transmittance in the visible and NIR regime.[26] At 100 mV s^{-1}, WO_3 exhibits a lower decrease in
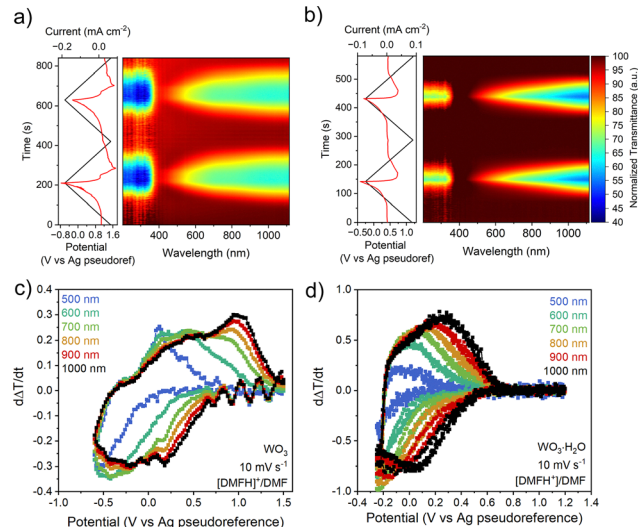
transmittance due to the lower degree of PICET (Fig. S14a). $WO_3 \cdot H_2O$ exhibits nonsynchronous optical changes, with low states of charge leading to transmittance decreases first in the NIR regime, and with continued reduction resulting in changes in the visible regime. This asynchronous transmittance change is associated with the impact of the structural water ligand on the electronic structure.[26] For $WO_3 \cdot H_2O$, the magnitude of the transmittance changes is maintained when cycled at 10 mV s^{-1} and 100 mV s^{-1} (Fig. 4b and Fig. S14b). UV-vis transmittance spectra at select potentials are shown in Fig. S15. The behavior in organic acid electrolytes is consistent with the response in aqueous inorganic acid electrolytes, which we attribute to the influence of the octahedral ligand environment in WO_3 vs. $WO_3 \cdot H_2O$ and the state of charge (n) accessible in each electrolyte at different scan rates.[26]

To further analyze the electrochromic responses in organic acid electrolytes, we quantified the rate of transmittance change, $d\Delta T/dt$, at wavelengths between 500 and 1000 nm. The $d\Delta T/dt$ vs., potential (Fig. 4c and d) correlates to the electrochemical current response in cyclic voltammetry for insertion hosts.[21,26] The response of WO_3 at 10 mV s^{-1} (Fig. 4c) shows that although the *operando* UV-vis data suggests a nearly simultaneous transmittance response across the wavelength range of interest, the rate of transmittance change is slightly larger at NIR wavelengths than in the visible regime. This effect is intensified at faster scan rates (Fig. S14c), as the transmittance rate of change at 500 nm becomes significantly weaker. The response of $WO_3 \cdot H_2O$ (Fig. 4d) shows a systematic increase in $d\Delta T/dt$ from 500 nm (visible) to 1000 nm (NIR). This wavelength-dependent optical modulation remains consistent even at faster scan rates (Fig. S14d), indicating that the electrochromic response of $WO_3 \cdot H_2O$ is less kinetically limited than in WO_3, in line with the CV results.

We characterized PICET into tungsten oxide thin films from non-aqueous electrolytes containing organic acids. We compared the PICET behavior of WO_3 and $WO_3 \cdot H_2O$ by electrochemically cycling the films in electrolytes containing organic acids ranging in pK_a from 5.07 to 19.35, finding that both oxides exhibit a near-Nernstian shift in the redox peaks. CV comparisons of aqueous inorganic acid and non-aqueous organic acid electrolytes show more sluggish PICET kinetics in the latter, which we hypothesize originate from the organic acid electrolyte and not the oxide electrodes. The response of $WO_3 \cdot H_2O$ was less medium-dependent, which we hypothesize occurs due to the Brønsted acidity of the $WO_3 \cdot H_2O$ which allows for more facile interfacial proton transfer in the absence of water in the electrolyte. Using *operando* electrochemical UV-vis-NIR spectroscopy, we observed transmittance changes across the visible and NIR wavelengths in both oxides upon reduction and oxidation in the organic-acid containing electrolytes, confirming the PICET mechanism. While WO_3 shows an almost simultaneous transmittance change across the visible and NIR regime, $WO_3 \cdot H_2O$ shows gradual changes in transmittance at lower states of charge only inducing NIR optical changes. To the best of our knowledge, this study provides the first report of electrochemical PICET from non-aqueous electrolytes into tungsten oxides.

Conflicts of interest

There are no conflicts to declare.

Data availability

Data for this article, including electrochemistry and UV-vis measurements, are available at Zenodo at https://doi.org/10.5281/zenodo.16903644.

Supplementary information is available. See DOI: https://doi.org/10.1039/d5cc04875c.

References

1 N. P. Holzapfel, V. Augustyn and V. Balland, *ACS Energy Lett.*, 2025, **10**, 1143–1164.
2 T. Takashima, K. Ishikawa and H. Irie, *ACS Catal.*, 2019, **9**, 9212–9215.
3 Y. Zhu, Z. He, Y. M. Choi, H. Chen, X. Li, B. Zhao, Y. Yu, H. Zhang, K. A. Stoerzinger, Z. Feng, Y. Chen and M. Liu, *Nat. Commun.*, 2020, **11**, 4429.
4 A. A. Fertig and E. M. Matson, *Inorg. Chem.*, 2022, **62**, 1958–1967.
5 K. R. Proe, E. Schreiber and E. M. Matson, *Acc. Chem. Res.*, 2023, **56**, 1602–1612.
6 S. E. Cooney, M. R. A. Walls, E. Schreiber, W. W. Brennessel and E. M. Matson, *J. Am. Ceram. Soc.*, 2024, **146**, 2364–2369.
7 S. Park, S. I. Nishimura, A. Kitada and A. Yamada, *ACS Appl. Energy Mater.*, 2024, **7**, 4347–4352.
8 H. S. Nedzbala, D. Westbroek, H. R. M. Margavio, H. Yang, H. Noh, S. V. Magpantay, C. L. Donley, A. S. Kumbhar, G. N. Parsons and J. M. Mayer, *J. Am. Chem. Soc.*, 2024, **146**, 10559–10572.
9 R. G. Agarwal, H. J. Kim and J. M. Mayer, *J. Am. Chem. Soc.*, 2021, **143**, 2896–2907.
10 H. Noh and J. M. Mayer, *Chem*, 2022, **8**, 3324–3345.
11 C. F. Wise and J. M. Mayer, *J. Am. Chem. Soc.*, 2019, **141**, 14971–14975.
12 N. Makivić, K. D. Harris, J. M. Tarascon, B. Limoges and V. Balland, *Adv. Energy Mater.*, 2023, **13**, 2203122.
13 T. Rocca, A. Gurel, D. Schaming, B. Limoges and V. Balland, *ACS Appl. Mater. Interfaces*, 2024, **16**, 23567–23575.
14 J. M. Mayer, *J. Catal.*, 2024, **439**, 115725.
15 J. B. Mitchell, N. R. Geise, A. R. Paterson, N. C. Osti, Y. Sun, S. Fleischmann, R. Zhang, L. A. Madsen, M. F. Toney, D. Jiang, A. I. Kolesnikov, E. Mamontov and V. Augustyn, *ACS Energy Lett.*, 2019, **4**, 2805–2812.
16 M. A. Spencer, N. P. Holzapfel, K. E. You, G. Mpourmpakis and V. Augustyn, *Chem. Sci.*, 2024, **15**, 5385–5402.
17 H. Li, M. Abdelgaid, J. R. Paudel, N. P. Holzapfel, V. Augustyn, J. R. McKone, G. Mpourmpakis and E. J. Crumlin, *J. Am. Chem. Soc.*, 2025, **147**, 6472–6479.
18 J. E. Benson, H. W. Kohn and M. Boudart, *J. Catal.*, 1966, **5**, 307–313.
19 M. Chagnot, S. Abello, R. Wang, J. Dawlaty, J. Rodríguez-López, C. Zhang and V. Augustyn, *J. Electrochem. Soc.*, 2025, **172**, 049002.
20 J. B. Mitchell, W. C. Lo, A. Genc, J. Lebeau and V. Augustyn, *Chem. Mater.*, 2017, **29**, 3928–3937.
21 J. Fortunato, B. Z. Zydlewski, M. Lei, N. P. Holzapfel, M. Chagnot, J. B. Mitchell, H. C. Lu, D. E. Jiang, D. J. Milliron and V. Augustyn, *ACS Photonics*, 2023, **10**, 3409–3418.
22 B. Z. Zydlewski, H. C. Lu, H. Celio and D. J. Milliron, *J. Phys. Chem. C*, 2022, **126**, 14537–14546.
23 S. Heo, C. J. Dahlman, C. M. Staller, T. Jiang, A. Dolocan, B. A. Korgel and D. J. Milliron, *Nano Lett.*, 2020, **20**, 2072–2079.
24 M. Duan, C. Hu, H. Li, Y. Chen, R. Chen, W. Gong, Z. Lu, N. Zhang, R. Long, L. Song and Y. Xiong, *JACS Au*, 2022, **2**, 1160–1168.
25 N. P. Holzapfel, M. Chagnot, P. S. Abdar, J. R. Paudel, E. J. Crumlin, J. R. McKone and V. Augustyn, *Chem. Mater.*, 2024, **36**, 11684–11696.
26 M. Chagnot, N. P. Holzapfel, L. Kollias, Y. Yue, G. Mpourmpakis and A. Veronica, *Phys. Rev. Mater.*, 2025, **9**, 085201.